EUKARYOTIC CELL, Feb. 2008, p. 223–236 Vol. 7, No. 2
1535-9778/08/$08.00+0 doi:10.1128/EC.00296-07

Iron Starvation and Culture Age Activate Metacaspases and Programmed Cell Death in the Marine Diatom *Thalassiosira pseudonana*▽

Kay D. Bidle* and Sara J. Bender†

Environmental Biophysics and Molecular Ecology Group, Institute of Marine and Coastal Sciences, Rutgers University, 71 Dudley Road, New Brunswick, New Jersey 08901

Received 13 August 2007/Accepted 13 November 2007

In the modern ocean, phytoplankton maintain extremely high primary production/biomass ratios, indicating that they bloom, die, and are replaced weekly. The molecular mechanisms regulating cellular mortality and turnover are largely unknown, even though they effectively short-circuit carbon export to the deep ocean and channel primary productivity to microbial food webs. Here, we present morphological, biochemical, and molecular evidence of caspase-mediated, autocatalytic programmed cell death (PCD) in the diatom *Thalassiosira pseudonana* in response to iron starvation. Transmission electron microscopy revealed internal degradation of nuclear, chloroplastic, and mitochondrial organelles, all while the plasma membranes remained intact. Cellular degradation was concomitant with dramatic decreases in photosynthetic efficiency, externalization of phosphatidylserine, and significantly elevated caspase-specific activity, with the addition of a broad-spectrum caspase inhibitor rescuing cells from death. A search of the *T. pseudonana* genome identified six distinct putative metacaspases containing a conserved caspase domain structure. Quantitative reverse transcription-PCR and Western blot analysis revealed differential gene and protein expression of *T. pseudonana* metacaspases, some of which correlated with physiological stress and caspase activity. Taken together with the recent discovery of the metacaspase-mediated viral infection of phytoplankton (K. D. Bidle, L. Haramaty, J. Barcelos-Ramos, and P. G. Falkowski, Proc. Natl. Acad. Sci. USA 104:6049–6054, 2007), our findings reveal a key role for metacaspases in the turnover of phytoplankton biomass in the oceans. Furthermore, given that Fe is required for photosynthetic electron transfer and is chronically limiting in a variety of oceanic systems, including high-nutrient low-chlorophyll regions, our findings provide a potential ecological context for PCD in these unicellular photoautotrophs.

Phytoplankton, or unicellular photoautotrophs that drift with the currents, represent the base of most marine food webs. Although they account for <1% of the Earth's biomass, they are responsible for nearly 50% of global annual carbon-based primary productivity (31). The steady-state maintenance of such a high production/biomass ratio implies that, on average, these organisms grow, die, and are replaced once every week (57). Substantial cell death via lysis documented in field populations of phytoplankton (1, 2, 14, 16, 58) challenges the long-held misconception among biological oceanographers that phytoplankton are immortal unless eaten by zooplankton grazers and highlights the importance of key death processes to marine ecosystems. Unfortunately, the mechanisms regulating phytoplankton cell death have received relatively little attention, even though they serve to couple primary production to microbial food webs (10), effectively short-circuiting carbon export to the deep ocean and stimulating upper ocean biogeochemical cycling (4, 10).

Autocatalytic cell death triggered by specific environmental stresses (e.g., cell age, nutrient deprivation, high light levels, oxidative stress, and UV exposure) in prokaryotic and eukaryotic unicellular phytoplankton (6, 10, 42, 51, 59) provides a mechanism to explain the high lysis rates independent of viral attack or grazing. This cellular self destruction is analogous to programmed cell death (PCD) in multicellular organisms, a form of autocatalytic cell suicide in which an endogenous biochemical pathway leads to apoptotic-like morphological changes and, ultimately, cellular dissolution. PCD involves the expression and biochemical coordination of specialized cellular machinery, such as receptors, adaptors, signal kinases, proteases, and nuclear factors. A specific class of intracellular cysteinyl aspartate-specific proteases, termed caspases, is of particular interest due to their ubiquitous role in both the initiation and execution of PCD through the cleavage of various essential proteins in response to proapoptotic signals (55).

The discovery of caspase homologues, paracaspases and metacaspases, in morphologically diverse organisms, including animals, higher plants, slime molds, unicellular protists, fungi, and bacteria (56), suggests that they may represent an ancestral core of executioners that led to the emergence of the cell death machinery. Presumably, early ancestors of plants and animals had minimal apoptotic machinery, with the more complex PCD systems in animals emerging with metazoans. While most metacaspase genes have been characterized only in silico, their genetic signatures have been directly linked to caspase activity in yeast (41) and trypanosomes (53). Their cellular roles, however, still remain an open question regarding unicellular protists and plants. Nonetheless, metacaspases (along with other putative PCD-related proteins) are widespread among prokaryotic and eukaryotic phytoplankton genomes

* Corresponding author. Mailing address: Environmental Biophysics and Molecular Ecology Group, Institute of Marine and Coastal Sciences, Rutgers University, 71 Dudley Road, New Brunswick, NJ 08901. Phone: (732) 932-6555, ext. 393. Fax: (732) 932-4083. E-mail: bidle@marine.rutgers.edu.

† Present address: School of Oceanography, University of Washington, Seattle, WA 98195.

▽ Published ahead of print on 26 November 2007.

(10), hinting at their early evolutionary development within these organisms. Furthermore, morphological and biochemical characteristics of caspase-mediated PCD have been observed in diverse phytoplankton lineages, including cyanobacteria, chlorophytes, and dinoflagellates (6, 42, 51, 59).

Diatoms are a class of unicellular phytoplankton with chromophyte lineage (29) that account for ~40% of total marine primary productivity in the modern ocean (47), including coastal and open-ocean upwelling zones (20, 28, 44, 45), warm oligotrophic gyres (18, 19), and the Southern Ocean (46). Since downward fluxes of biogenic silica and organic matter in the modern ocean derive largely from diatom productivity (40, 47, 50), there is increased interest in the mechanistic processes that regulate their fate. Indeed, the physiological state and life history of diatom assemblages dictate whether diatom Si and its associated organic C are either recycled in the euphotic zone or exported to depth (8, 9, 17), placing mechanistic importance on cellular processes mediating the bloom-to-post-bloom transition.

Autocatalytic cell death in diatoms was first documented in *Ditylum brightwellii* (15) and *Thalassiosira weissflogii* (5) in response to nutrient limitation, with the latter study reporting the activation of unknown proteases. More recently, a threshold and dose-dependent response to secondary metabolites elicited from diatoms during stress, such as the aldehyde 2-*trans*, 4-*trans*-decadienal, was shown to induce morphological and biochemical features of apoptosis (22). Subsequently, Vardi et al. (61) demonstrated a stress surveillance and cell-cell communication system in *Phaeodactylum tricornutum* that employs secondary messengers (e.g., nitric oxide and calcium) to critically regulate PCD and cell fate. A novel calcium-regulated protein (ScDSP), with a transmembrane domain and a pair of EF-hand motifs, also was identified recently in the diatom *Skeletonema costatum* and shown to have strong up-regulation of gene expression in dying cells, suggestive of a role in the signal transduction of stress to the death machinery (24). These studies have provided intriguing mechanistic insights into how diatoms couple environmental stress levels with cell death. Nevertheless, we still have very little mechanistic insight into the biochemical execution of autocatalytic cell death in diatoms, especially its relationship to caspase-mediated PCD.

Here, we investigate the activation of autocatalytic PCD in the diatom *Thalassiosira pseudonana* as a central death pathway in response to nutrient starvation. *T. pseudonana* is representative of natural diatom populations and is an excellent model system to elucidate molecular signatures of PCD, given its completed genome sequence (3). We specifically examine the presence of metacaspase genes in *T. pseudonana*, their expression in response to physiological stress, and their potential role in the implementation of PCD.

MATERIALS AND METHODS

Culture maintenance and sampling. *Thalassiosira pseudonana* (strain CCMP 1335) was obtained from the Provasoli-Guillard Culture Collection for Marine Phytoplankton (Bigelow Laboratory for Ocean Sciences, ME). Liquid batch cultures of *T. pseudonana* were grown in f/2 medium and incubated at 18°C under a 14-h light/10-h dark illumination regimen at 100 microeinsteins m^{-2} s^{-1} with constant bubbling (33). The light intensity was measured using a Li-Cor quantum/radiometer/photometer (model LI-189).

For experimental setup, a starter culture of *T. pseudonana* was grown in f/2 medium to late exponential phase (~2.0×10^6 cells ml^{-1}), after which the cells were pelleted via centrifugation (10,000 × *g*, 18°C, 10 min) and washed once in an equal volume of autoclaved (0.2-μm filter pore size) filtered seawater in order to remove residual medium. Washed cells were used to inoculate 3-liter treatments of modified or replete f/2 medium. The initial cell concentration of each culture treatment was 1.5×10^5 cells ml^{-1}. Culture treatments consisted of replete f/2 medium (883 μM nitrate, 107 μM silicate, 36 μM phosphate, and 10 μM iron) and f/2 medium without added iron (Fe starved).

Triplicate samples were removed daily from each culture and monitored for a variety of physiological parameters. Growth and cell abundance were determined using a Coulter multisizer II (Beckman Coulter). Sample volumes (500 μl) were counted using a 70-μm orifice diameter. The maximum photochemical quantum yield of photosystem II (variable fluorescence/maximum fluorescence ratio [F_v/F_m]) was determined using the fluorescence induction and relaxation system (FIRe; Satlantic Instrument) as an indication of photosynthetic health (38). Cell pellets also were collected via centrifugation for subsequent biochemical and molecular biological analyses. Pellets were frozen immediately in liquid nitrogen and stored at −80°C until processing.

TEM. The internal cell morphology of *T. pseudonana* cells was examined using transmission electron microscopy (TEM). Cells were pelleted via centrifugation (10,000 × *g*, 4°C, 5 min) and resuspended in 500 μl Trump's EM fixative (4% formaldehyde, 1% glutaraldehyde in phosphate buffer, pH 7.2) overnight at 4°C. Cells were rinsed once, resuspended in phosphate-buffered saline (PBS; pH 7.5), and stored at 4°C for <1 week. Fixed cells were rinsed three times for 15 min in Milloning's phosphate buffer, pH 7.3, postfixed for 2 h in 1% buffered OsO_4, washed three times, and dehydrated through a graded series of ethanol. After the replacement of ethanol with propylene oxide, cells were embedded in an Epon-Araldite cocktail. Sections were cut using an LKB 2088 ultramicrotome, collected on 200-mesh copper grids, and stained with uranyl acetate and lead citrate. The stained sections were visualized and photographed using a JEM-100CXII electron microscope.

Measurements of caspase activity. Cells were resuspended in caspase activity buffer {50 mM HEPES (pH 7.3), 100 mM NaCl, 10% sucrose, 0.1% 3-[(3-cholamidopropyl)-dimethylammonio]-1-propanesulfonate, and 10 mM dithiothreitol} and sonicated on ice (four times, each for a 30-s $cycle^{-1}$) using an ultra cell disruptor (Microson) set at power level 2. Cell extracts were centrifuged (10,000 × *g*, 2 min), and supernatant was transferred into triplicate microtiter plate wells containing the fluorogenic, peptide substrate for caspase-8, Ile-Glu-Trp-Asp-7-amido-4-trifluoromethylcoumarin (IETD-AFC; Calbiochem) at a 50 μM final concentration. The hydrolysis of the substrate for caspase 3, Asp-Glu-Val-Asp-AFC (DEVD-AFC), also was tested. Purified recombinant human caspase 8 was purchased commercially (BioMol) and served as a positive control for activity (10 ng $assay^{-1}$). This caspase 8 was derived from human cDNA encoding residues identical to residues Ser-217 to Asp-479 (C terminus; Swiss-Prot accession no. Q14790) and expressed in *Escherichia coli*. A mixture of activity buffer and IETD-AFC served as a negative control. A kinetic analysis was performed for substrate cleavage (excitation, 400 nm; emission, 505 nm) over a 2-h period with measurements taken at 10-min intervals using a Spectra Max Gemini XS plate reader (Molecular Devices) and the SoftMax Pro 3.1.1 analysis program. Cleavage rates were normalized to protein, as determined by the bicinchoninic acid protein assay kit (Pierce).

The broad-spectrum caspase inhibitor z-Val-Ala-Asp-fluromethylketone (z-VAD-FMK) was added to cell extracts prior to the addition of IETD-AFC in caspase activity assays to test for the elimination of caspase activity. The inhibitor also was added to Fe-starved cultures (final concentration, 20 μM) to test for its effect on in vivo cell physiology. Since z-VAD-FMK was dissolved in dimethyl sulfoxide (DMSO), DMSO-only additions (0.1% final concentration) were run in parallel as controls. The Fe concentration in the inhibitor was determined by medium resolution and inductively coupled plasma mass spectrometry (ICP-MS; Finnigan Element 2) at the Rutgers Inorganic Analytical Laboratory and compared to DMSO and duplicate procedural blanks in order to detect trace Fe contamination. Equal volumes (10 μl) of DMSO-reconstituted inhibitor (220 nmol) and DMSO were digested overnight with 250 μl of 50% quartz-distilled nitric acid (Q-HNO_3) in 3-ml Teflon bombs for 12 h on a hotplate. Digests were dried and reconstituted in 1 ml 5% Q-HNO_3. Each procedural blank consisted of a 50% Q-HNO_3 digest followed by reconstitution in 1 ml 5% Q-HNO_3. Samples were spiked with a Y internal standard prior to ICP-MS analysis.

In situ detection of PCD markers. Cells were stained in vivo with a fluorescein isothiocyanate (FITC) conjugate of z-VAD-FMK to visualize cells containing activated caspases (CaspACE; Promega Corporation, Madison, WI). Cells were pelleted via centrifugation (10,000 × *g*, 10 min, 4°C), washed once with PBS (pH 7.5), and resuspended in PBS prior to the addition of CaspACE (final concentration, 20 μM). Cells were stained for 20 min at 18°C in the dark, after which they were pelleted via centrifugation, washed once with PBS, fixed with 2%

formalin–PBS, and stored at 4°C until analyzed (within 1 week). An unstained control was performed at each time point for comparison.

Staining with Annexin V-FITC (Invitrogen-Molecular Probes) was used as an in vivo test for phosphatidylserine (PTS) externalization, a diagnostic marker of PCD. Cells were harvested via centrifugation, resuspended in 100 μl of Annexin binding buffer (10 mM HEPES, 140 mM NaCl, and 2.5 mM CaCl2, pH 7.4), and stained with 10 μl of Annexin V for 20 min at room temperature in the dark. After being stained, cells were pelleted via centrifugation, washed once with PBS, resuspended in 2% formalin–PBS, and stored at 4°C until further analysis.

Stained cells were visualized and photographed by differential interference contrast and epifluorescence microscopy using an IX71 inverted microscope (Olympus) and a Retiga Exi SVGA high-speed monochromatic cooled charge-coupled-device camera (QImaging) interfaced with iVision acquisition/image analysis software (version 4.0; BioVision Technologies). Samples also were quantified by flow cytometry using a Beckman Coulter Cytomics FC500 flow cytometer (Flow Cytometry Core Facility, Environmental and Occupational Health and Safety Institute, Rutgers University). An unstained control was used for each sample set (i.e., for each sampling time and treatment) to gate *T. pseudonana* cells based on side scatter (size) and forward scatter (granularity) and to correct for background FITC fluorescence. Five thousand cells were counted for each sample.

Metacaspase identification. Metacaspase genes were identified in the *T. pseudonana* genome using annotated gene models (DOE Joint Genome Institute; http://genome.jgi-psf.org/Thaps3/Thaps3.home.html) and confirmed by performing a translation BLAST (tBLASTn) with a known metacaspase protein from *Saccharomyces cerevisiae* (ScMca-1) (41). A subsequent protein BLAST (BLASTp) search was performed in GenBank for each putative metacaspase protein in order to determine the identity of the closest match and to look for the presence of conserved domains (COGs) (NCBI; http://www.ncbi.nlm.nih.gov/). Multiple metacaspase protein alignments were performed with Clustal W using the Vector NTI package. Protein targeting predictions were assessed using the TargetP, version 1.1, server (http://www.cbs.dtu.dk/services/TargetP/).

Western blot analysis. Frozen cells were resuspended in a mixture of PBS and protease inhibitor cocktail (Sigma), sonicated, and centrifuged (16,000 × *g*, 1 min). Supernatants were loaded with equal amounts of protein onto 15% Criterion Tris-HCl polyacrylamide gels (Bio-Rad), subjected to sodium dodecyl sulfate (SDS)-polyacrylamide gel electrophoresis (200 V, 1.5 h), and transferred onto polyvinylidene difluoride membranes (100 V, 1 h). Transfer buffer consisted of (per 500 ml of MilliQ water) 15.0 g Tris base, 72.0 g glycine, and 5.0 g SDS. Membranes were probed with polyclonal antisera raised against a purified, recombinant metacaspase protein from *Emiliania huxleyi* (EhMC; titer, 1:500) (11), preimmune antisera (collected from the same rabbits prior to injection with purified EhMC; 1:500), or polyclonal antisera to purified recombinant *T. pseudonana* manganese superoxide dismutase (Mn-SOD; titer, 1:3,000) (64). Polyclonal goat anti-rabbit immunoglobulin G (IgG) horseradish peroxidase (HRP) (titer, 1:10,000; Pierce) and an HRP chemiluminescent substrate (Bio-Rad) was used for detection. Cell extracts from *E. huxleyi* (10 μg total protein lane^{-1}) and commercial recombinant human caspase 8 (10 ng lane^{-1}; BioMol) served as controls. Hybridization with the anti-rabbit IgG HRP secondary antibody controlled for nonspecific binding.

qRT-PCR. DNA oligonucleotide primers were designed for each *T. pseudonana* metacaspase (TpMC) gene using the PrimerQuest tool (Integrated DNA Technologies; http://www.scitools.idtdna.com/Primerquest/). An additional primer set was designed for actin, which served as a housekeeping gene and a normalizer for quantitative real-time PCR (qRT-PCR) analyses of RNA expression (54). Primer sequences were designed within exon coding regions for all genes (Table 1).

Metacaspase gene fragments were amplified from genomic DNA, cloned into a PCR-compatible cloning vector (pCR4.0 TOPO; Invitrogen), and transformed into TOP 10-competent *E. coli* cells (Invitrogen). Actin amplicons were cloned into pCR2.1-TOPO (Invitrogen). Upon confirmation of positive clones, plasmid DNA was purified using a commercial plasmid DNA preparation kit (Qiagen) and linearized via a restriction enzyme digestion (PstI for metacaspase clones, NcoI for actin clones) according to the manufacturer's protocol (Promega).

Linear plasmid DNA and primer sets were used to determine optimal PCR conditions, including forward primer/reverse primer ratios, $MgCl_2$ concentration, and total primer concentration. Optimization procedures were necessary in order to provide confidence in maximal PCR amplification. Once all conditions were optimized, standard curves were generated using serially diluted linear plasmid DNA for each gene. Optimal conditions were taken to be the lowest amplification threshold cycle in combination with minimal primer dimers. The Stratagene two-step brilliant qRT-PCR core reagent kit was used to optimize each of the primer sets to an amplification efficiency above 85%. Quantitative PCR progression was monitored using the intercalating dye Sybr green I on a Stratagene MX 3000P instrument.

TABLE 1. Primer sequences used to monitor gene expression in *T. pseudonana*

Primer name[a]	Primer sequence[b] (5′–3′)
TpMC1, 507F	TGTCCTCATGGATGATGGAGAGCA
TpMC1, 729R	ATCATCGCGAATCATACCAGCCGA
TpMC2, 11F	TTCCTAATACACCACGCGGTTCCA
TpMC2, 473R	AACGCAATCAAACGACAGCCTTCC
TpMC3, 865F	ACACAACGTGCAGTGTTGATTGGG
TpMC3, 1149R	TTCGTCGCCGTTATCGTCCTTGAT
TpMC4, 101F	ATGGGCAGACTTGCTACGGAAGAT
TpMC4, 569F	AGGAACCAAAGCCTCGTCGTAACT
TpMC5, 29F	AATCCTTCGGGTACAAAGAGGGCA
TpMC5, 357R	AATCCGCCGGTATCAAAGTCTCGT
TpMC6, 57F	TTACGTCGGACAGCAAGGTCAACT
TpMC6, 451R	AATGACAGCAATCCATCAACGCCG
Actin, 235F[c]	ACCAACTGGGACGACATGGAGAAA
Actin, 490R	TGTGGGTAACACCATCTCCCGAAT

[a] Numbers after the TpMC designation refer to the location on the transcript.
[b] Primers were designed using the Primerquest tool (Integrated DNA Technologies; http://www.scitools.idtdna.com/Primerquest) and refer to genes listed in Table 2.
[c] Used as a housekeeping gene (Protein ID 25772 [ACT1] from the database at http://genome.jgi-psf.org/Thaps3/Thaps3.home.html).

RNA extraction and gene expression analysis. The expression of each TpMC gene was analyzed using qRT-PCR for triplicate samples collected from replicate cultures. Total RNA was extracted using TRIzol reagent (Invitrogen), and contaminating DNA was removed with Turbo DNase treatment (Ambion), both according to the manufacturers' protocols. Additional DNase was added to samples, which contained more than 200 μg ml^{-1} RNA. One microliter of DNase was added every 30 min over a 1.5-h incubation period. RNA was quantified after DNase treatment. A first-strand cDNA synthesis kit utilizing 50 μM oligo(dT) primers was used to generate cDNA (Stratagene). Equal concentrations of RNA were loaded into the first-strand reaction, and 1 μl of cDNA was loaded into each subsequent qRT-PCR. Gene expression was determined using a relative quantification protocol in the MX300P software package (Stratagene). The expression of target metacaspase genes was normalized to actin and calibrated to an initial time point (1 day). Calculations incorporated individual gene amplification efficiencies. Reactions either containing no template or containing DNase-treated RNA (without an RT reaction) as the template were run for each gene and served as negative controls.

RESULTS

Physiological response to culture age and iron starvation. Fe starvation triggered acute physiological stress, with cultures reaching a relatively low maximum cell concentration of 8.6×10^5 cells ml^{-1} on day 3 before rapidly declining by 90% to 6.8×10^3 cells ml^{-1} on day 7 (Fig. 1A). The replete treatment displayed more extensive and sustained growth, reaching a peak cell concentration of 2.3×10^6 cells ml^{-1} after 4 to 5 days. After this point, the cell abundance declined with a mortality rate of 0.13 to 0.79 day^{-1}.

The F_v/F_m was monitored as a measure of photosynthetic health. Both cultures started with an F_v/F_m of ~0.5 (Fig. 1B), indicative of healthy photosystem II photochemistry. F_v/F_m in the Fe-starved treatment declined steadily over the experimental time period, dropping by 46% to 0.16 at day 6, after which it remained at ~0.1 (Fig. 1B). Replete cells maintained an F_v/F_m of >0.4 for the first 5 days, after which it dropped to ~0.1, concomitant with declining cell numbers.

Caspase activity. Decreases in cell abundance and F_v/F_m coincided with steady increases in caspase-specific activity, as

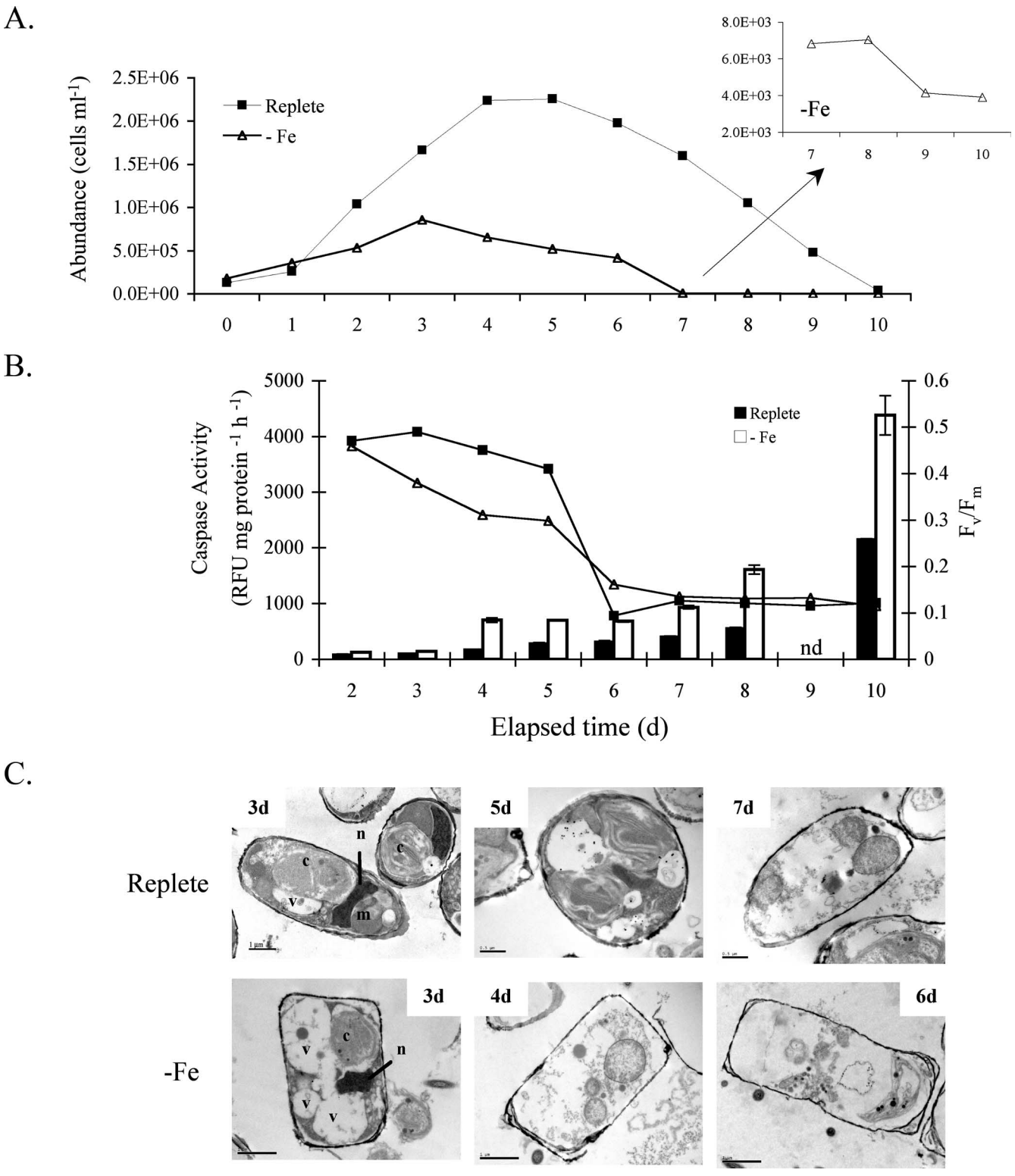

FIG. 1. Physiological response of *T. pseudonana* to culture age and Fe starvation. (A) Time course of cell abundance showing the growth and subsequent crash of batch cultures incubating in replete medium or Fe-starved medium. (B) Caspase-specific activity (bars) and photosynthetic efficiency of photosystem II (lines) during the same time period. Error bars represent the standard deviations of technical triplicates. The experiment shown is typical of three experiments. Where not visible, error bars are smaller than the symbols. (C) TEMs of cells incubated in each condition and illustrating morphological changes at the selected time points. The elapsed time (in days) is indicated in the top corner of each panel. Scale bars, 1 μm. d, day; n, nucleus; m, mitochondria; c, chloroplast; and v, vacuole.

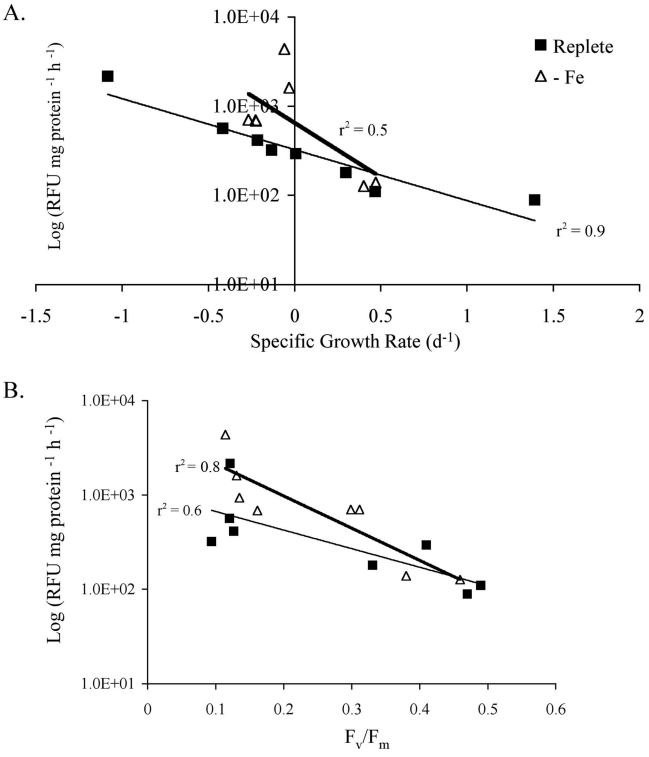

FIG. 2. Relationship between caspase activity and specific growth rate (A) or F_v/F_m (B) for aging (thin line) and Fe-starved cultures (thick line). Linear regressions were performed with the indicated correlation coefficients. (A) For aging cultures, $y = 325.9e^{-1.3163x}$; for Fe-starved cultures, $y = 567.28e^{-2.7396x}$. (B) For aging cultures, $y = 1055.4e^{-4.5382x}$; for Fe-starved cultures, $y = 4827.6e^{-7.9256x}$). d, day.

measured by the cleavage of IETD-AFC. Caspase-specific activity increased by 24- and 35-fold over the 10-day time course for replete and Fe-starved treatments, respectively. Fe starvation consistently triggered higher caspase activity at each respective sampling time, with activity peaking on day 10 at >4,000 relative fluorescence units (RFU) mg protein^{-1} h^{-1}. DEVD-AFC hydrolysis rates also were elevated over this time period, but they ranged from only 31 to 54% and 26 to 40% of that of IETD-AFC hydrolysis in Fe-starved and replete treatments, respectively. Caspase activation in *T. pseudonana* showed a dependence on photosynthetic stress (low F_v/F_m) and mortality rate (Fig. 2); linear regressions yielded r^2 values of >0.5 for all treatments, with Fe-starved cells displaying steeper slopes.

Internal morphological characteristics. TEM analysis detected distinct, internal morphological changes in each culture condition (Fig. 1C). Cells collected during a period of exponential growth (day 3) were characterized by generally high electron density and organized, distinct, compact organelles, including a nucleus, chloroplasts with well-defined thylakoid membranes, mitochondria, and nutrient storage vacuoles. Defined organelles were still visible in the replete culture after 5 days, but by 7 days there was clear internal degradation characterized by the lack of recognizable organelles and empty regions of low electron density, all while cell membranes remained intact.

Fe-starved cells were characterized by more dramatic vacuolization and internal degradation, coincident with decreases in cell abundance and F_v/F_m and increases in caspase-specific activity. Most cells lacked the most recognizable organelles by day 4 and appeared empty by day 6 (Fig. 1C, bottom panels). Genomic DNA degradation was observed as a smear on agarose gels during this time period (data not shown), consistent with massive internal organelle degradation via TEM. In each case, cells generally contained intact cell membranes, with no visual evidence of cell lysis.

In vivo staining for PCD markers. Staining of *T. pseudonana* cells with CaspACE and Annexin V-FITC was most prominent for photosynthetically unhealthy cells, identified by their weak, red chlorophyll fluorescence (Fig. 3A and B). A relatively small percentage of cells was positively stained in Fe-starved cultures at early time points (2 days); 2.1 and 14.8% of cells were stained with Annexin V and CaspACE, respectively (Fig. 3C and D). Staining increased markedly at later time points, reaching 61.6 and 73.1% after 7 days for Annexin V and CaspACE, respectively, as illustrated by a clear shift in the cell population toward increased fluorescence (approximately fivefold) (Fig. 3C and D). The percentage of positively stained *T. pseudonana* cells, quantified by flow cytometry, was dramatically elevated in Fe-starved cultures over time (Fig. 3E), with both stains generally paralleling each other in timing and extent. The percentage of CaspACE-stained cells increased from 10.4 (day 3) to 73.1% (day 7) (staining was not measured on day 8), while the percentage of Annexin V-FITC-stained cells increased from 10.8 to 61.6% over the same time period. Even though there was a slight increase during the course of the experiment, the degree of staining for replete cells was noticeably lower, remaining at <20%.

Effect of caspase inhibition. The addition of the caspase inhibitor z-VAD-FMK to Fe-starved cells reduced cellular caspase activity by 97 and 91% after 1 and 2 days, respectively, compared to the activity of the DMSO-only and untreated Fe-starved cells (Fig. 4, inset). Inhibitor treatment rescued cells from death and triggered a marked increase in *T. pseudonana* cell abundance to 2×10^6 cells ml^{-1} (day 1) and $>3.0 \times 10^6$ cells ml^{-1} (day 2), corresponding to specific growth rates of 0.5 to 0.6 day^{-1}. The increases in growth upon the addition of z-VAD-FMK resulted in a surplus of 1.8×10^6 to 2.4×10^6 cells ml^{-1} at 1 to 2 days, very low caspase activity, and raised F_v/F_m from 0.281 to 0.475. In contrast, cell abundance in both the DMSO-only and untreated cultures peaked at $\sim 1.0 \times 10^6$ cells ml^{-1} and subsequently decreased after 1 to 2 days, with both cultures exhibiting low (0.09 to 0.19) or negative growth rates (−0.05 to −0.99), elevated caspase-specific activity (>1,200 RFU mg protein^{-1} h^{-1}), and low F_v/F_m (0.227 to 0.295) (Fig. 4). The observed physiological response to z-VAD-FMK addition was not due to Fe contamination. Measured Fe concentrations in the z-VAD-FMK caspase inhibitor stock and DMSO were identical and very low (<0.1 ppm). Potential Fe carryover from the DMSO and inhibitor spikes was calculated to be 1.7 nM, far lower than the 88 nM minimum required to account for the observed growth, based on measured cellular iron quotas in *T. pseudonana* of 40 amol cell^{-1} (39).

Metacaspase identification. Six metacaspase genes were identified in the *T. pseudonana* genome with putative molecular masses ranging from 17.8 to 52.4 kDa (Table 2). Expressed

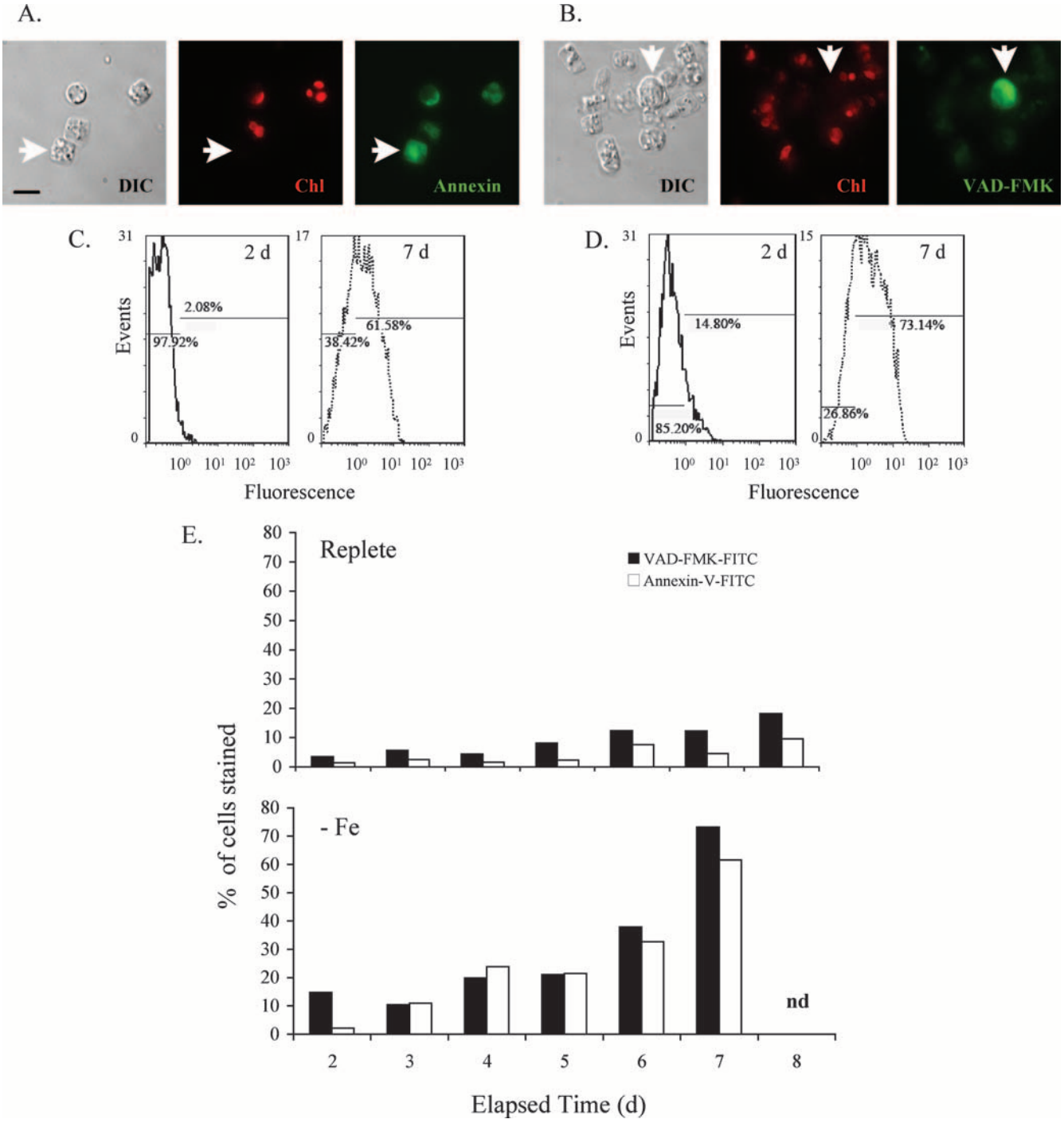

FIG. 3. In vivo detection of PCD markers in *T. pseudonana*. (A, C) Staining for the externalization of PTS using Annexin V-FITC. (B, D) Staining for caspase activity using z-VAD-FMK–FITC. (A, B) Differential interference contrast micrographs (DIC) detailing the cell structure and epifluorescence micrographs demonstrating cellular fluorescence due to chlorophyll (Chl) or PCD stains (Annexin V and z-VAD-FMK). Arrows indicate positively stained cells. (C, D) The relative fluorescence distributions of Fe-starved cells sampled at 2 and 7 days, as determined by flow cytometry (5,000 cells were counted). (E) Comparison of Annexin V and CaspACE staining for replete and Fe-starved cultures during an 8-day time course. nd, not determined; d, day.

sequence tags (EST) have been detected for the predicted metacaspases (43), but we note that not all current gene models have been verified experimentally. TpMC proteins were most similar to metacaspase-like proteins from various fungi, including *Aspergillus fumigatus* Af293, *Coprinopsis cinerea okayama* 7#130, *Neurospora crassa* OR74A, and *Pichia stipitis* CBS 6054, as well as the higher plant *Vitis vinifera*; E values ranged from 4 E^{-24} to 9 E^{-44} (Table 2). A conserved pepti-

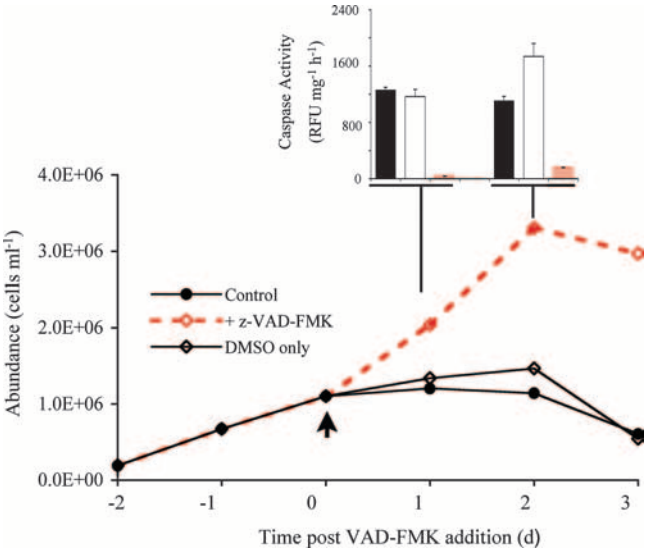

FIG. 4. Response of cell abundance and caspase-specific activity (inset) to the addition of z-VAD-FMK (arrow) to an Fe-starved culture. Caspase activity was measured after the addition on days 1 and 2 to determine the effectiveness of the inhibitor. Error bars represent the standard deviations of measurements from triplicate samples. For cell abundance data, error bars are smaller than the symbols. d, day.

dase_C14 caspase domain (pfam00656) was detected in each TpMC (E values of 6 E^{-12} to 6 E^{-25}). In addition, TpMC2 and TpMC5 contained an uncharacterized protein-containing caspase domain (COG4249) (Table 2). Multiple alignments of the six TpMC proteins with metacaspases from *A. fumigatus* Af293, *S. cerevisiae*, and the marine coccolithophore *E. huxleyi* confirmed amino acid identities around cysteine-histidine catalytic active-site regions characteristic of caspase-like proteins (Fig. 5). Protein target analyses (using TargetP, version 1.1) predicted that TpMC3 contains a chloroplast transit peptide and is targeted to the chloroplast, with a probability of 0.943 and a reliability class of 1. A similar analysis predicted that TpMC2 is targeted to the mitochondria, although at a lower probability (0.614) and reliability class (4). All other metacaspases showed no apparent organelle targeting.

Metacaspase and Mn-SOD protein expression. Western blot analysis of *T. pseudonana* cell extracts collected from replete or Fe-starved cultures (Fig. 6A) revealed immunohybridization of distinct proteins to a polyclonal antibody raised against a purified, recombinant 36-kDa EhMC (Fig. 6B). Hybridizing proteins in *T. pseudonana* ranged in size from ~17 to ~50 kDa and corresponded to putative molecular masses of all identified TpMC proteins (Table 2). The most intense immunohybridization occurred with an ~50-kDa protein(s) in exponentially growing cells at early time points in both culture treatments (Fig. 6B, band a; Fig. 6D). This band persisted for up to 10 days in the replete culture but disappeared in the Fe-starved culture after 5 days. Intense early expression also was seen for an ~17-kDa protein in both treatments, eventually disappearing after 4 days (Fig. 6B, band b). Faint immunohybridization was observed with ~20-kDa proteins at 3 to 4 days for Fe-starved cells (Fig. 6B, bands c and d). The disappearance of the 50- and 17-kDa bands was marked by the appearance of distinct ~37-kDa (band e) and ~25-kDa (band f) proteins, with the latter being in the Fe-starved culture only. The expression of these proteins was linked with cell death and marked increases in caspase-specific activity (Fig. 6D).

The EhMC polyclonal antibody displayed strong, specific immunohybridization to a ~36-kDa protein in *E. huxleyi* cell extracts, corresponding with the purified, recombinant EhMC protein size used to generate the antibody. Strong hybridization also was observed for the expected 18- and 12-kDa bands characteristic of purified, recombinant human caspase 8 (Fig. 6B). No hybridization was detected when *T. pseudonana* cell extracts were incubated with preimmune rabbit antisera or the anti-rabbit IgG HRP conjugate (not shown).

The same cell extracts were probed with a polyclonal antiserum against Mn-SOD from *T. pseudonana* in order to determine if cells were experiencing oxidative stress (Fig. 6C). The only hybridization observed in both Fe-starved and replete cell extracts was to the ~25-kDa Mn-SOD (64). Mn-SOD was consistently upregulated in Fe-starved cell extracts from all

TABLE 2. Metacaspase genes in *T. pseudonana* showing the closest BLAST matches and conserved domains

Protein ID[a]	Abbreviation (this study)	Putative molecular mass[b] (kDa)	Best BLAST hit[c] (accession no.); E value	Conserved domain(s) (E value)
270038	TpMC1	35.2	Hypothetical protein CCIG_08798, *Coprinopsis cinerea okayama*7#130 (EAU92175); 3 E-38	pfam00656, peptidase_C14 caspase domain (6 E-17)
36443	TpMC2	23.1	Predicted protein, *Pichia stipitis* CBS 6054 (XP_001386423); 1 E-43	pfam00656, peptidase_C14 caspase domain (6 E-25); COG4249, uncharacterized protein containing caspase domain (5 E-3)
2505	TpMC3	52.4	Hypothetical protein, *Neurospora crassa* OR74A (XP_959720); 2 E-41	pfam00656, peptidase_C14 caspase domain (2 E-16)
268857	TpMC4	38.8	Hypothetical protein, *Vitis vinifera* (CAN66365); 4 E-24	pfam00656, peptidase_C14 caspase domain (9 E-15)
270007	TpMC5	26.5	Metacaspase CasA, *Aspergillus fumigatus* Af293 (XP_750419); 2 E-26	pfam00656, peptidase_C14 caspase domain (6 E-12); COG4249, uncharacterized protein containing caspase domain (4 E-3)
38187	TpMC6	17.8	Metacaspase CasA, *Aspergillus fumigatus* Af293 (XP_750419); 9 E-44	pfam00656, peptidase_C14 caspase domain (1 E-16)

[a] http://genome.jgi.psf.org/Thaps3/Thaps3.home.html.
[b] Based on the translated protein sequence of the gene model.
[c] http://www.ncbi.nlm.nih.gov/.

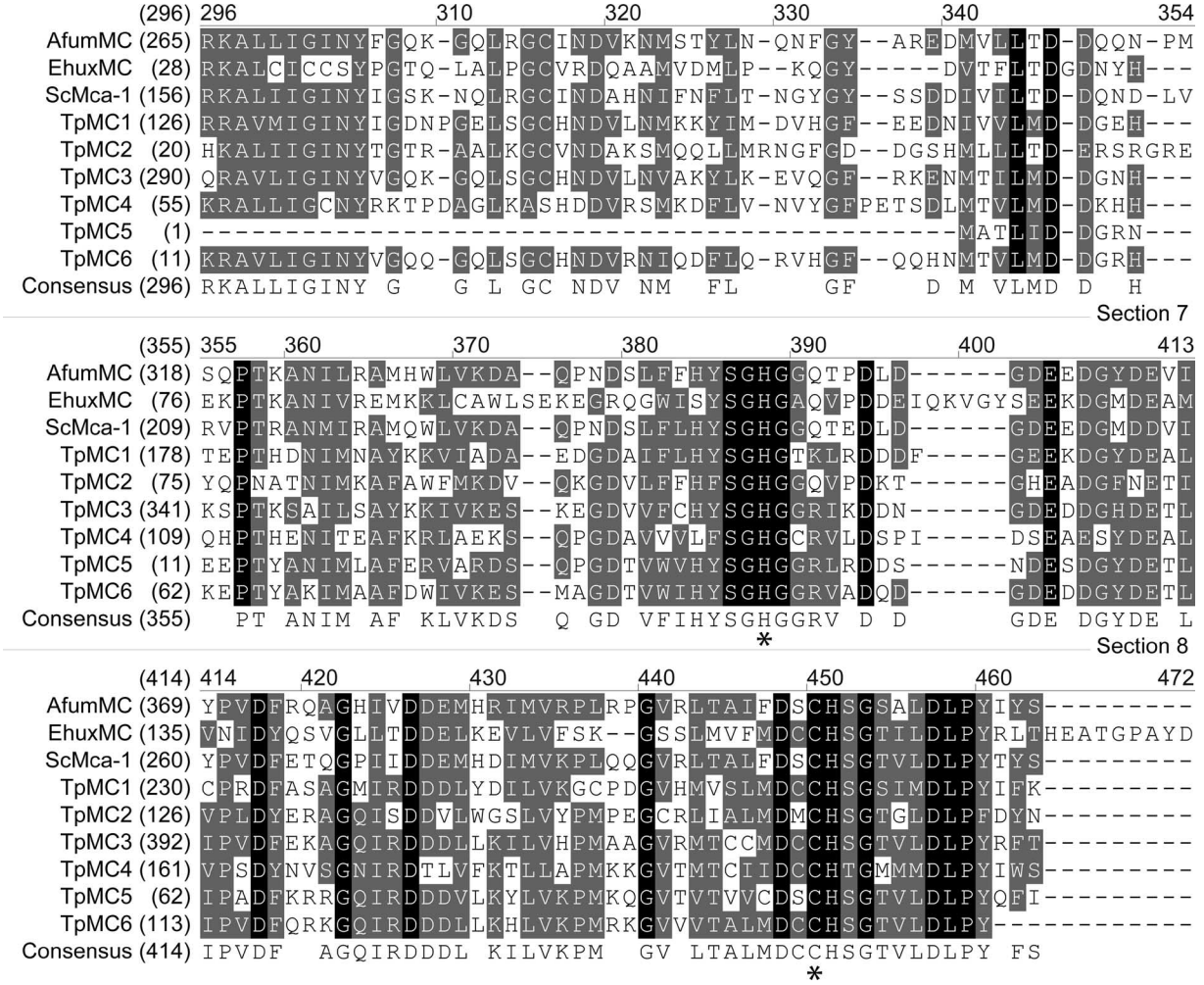

FIG. 5. Partial alignment of the TpMC protein sequences with metacaspases from *E. huxleyi*, *S. cerevisiae*, and *A. fumigatus* showing significant amino acid similarity, especially in the conserved, histidine-cysteine catalytic diads (indicated by asterisks). Sequences were aligned using Clustal W within the Vector NTI package. Abbreviations: EhuxMC, *E. huxleyii* metacaspase; ScMca-1, *S. cerevisiae* metacaspase; and AfumMC, *A. fumigatus* metacaspase. Black shading, identical residue; gray shading, conserved amino acid residue.

time points, indicative of chronic oxidative stress. In contrast, cell extracts from healthy, actively growing replete cells had low-level expression of Mn-SOD, with expression greatly increasing as cells reached stationary and death phases, diagnostic of elevated levels of reactive oxygen species (ROS) (Fig. 6D).

Metacaspase gene expression. We also assessed the expression of individual TpMC genes in the same cell extracts (Fig. 7). Distinct differences were observed in the extent and pattern of TpMC gene expression for replete and Fe-starved cultures. Gene expression was detected for TpMC1, TpMC3, TpMC4, TpMC5, and TpMC6 in replete cultures (Fig. 7), with most genes being downregulated relative to initial day 1 levels. Only TpMC4 expression was elevated (more than twofold at 5 days). TpMC2 transcripts were not detected in replete cultures. All TpMC genes were expressed in Fe-starved cells, with several TpMC genes being upregulated, especially at later time points (>5 days), as cells displayed physiological stress and mortality (Fig. 6C). TpMC2 and TpMC4 expression were upregulated up to threefold after 5 to 6 days, coincident with cell death and caspase activation (Fig. 6C). TpMC5 and TpMC6 also were slightly upregulated at early time points (<5 days) but subsequently dropped below day 1 levels. TpMC1 and TpMC3 were consistently downregulated in Fe-starved cells by as much as three- to fourfold.

DISCUSSION

The primary goal of this study was to investigate the activation and execution of autocatalytic PCD in the model diatom *Thalassiosira pseudonana*. Previous studies have documented autocatalytic cell death in diatoms in response to nutrient limitation (5, 15) characterized by the activation of unidentified proteases (5), but detailed mechanistic insights into the identity of induced proteases and the relationship of autocatalytic cell death to caspase-mediated PCD remain unknown. We utilized *T. pseudonana* as a model system to elucidate the morphological and biochemical characteristics of autocatalytic PCD in diatoms in response to nutrient stress and culture age. Not only is *T. pseudonana* represented in natural diatom pop-

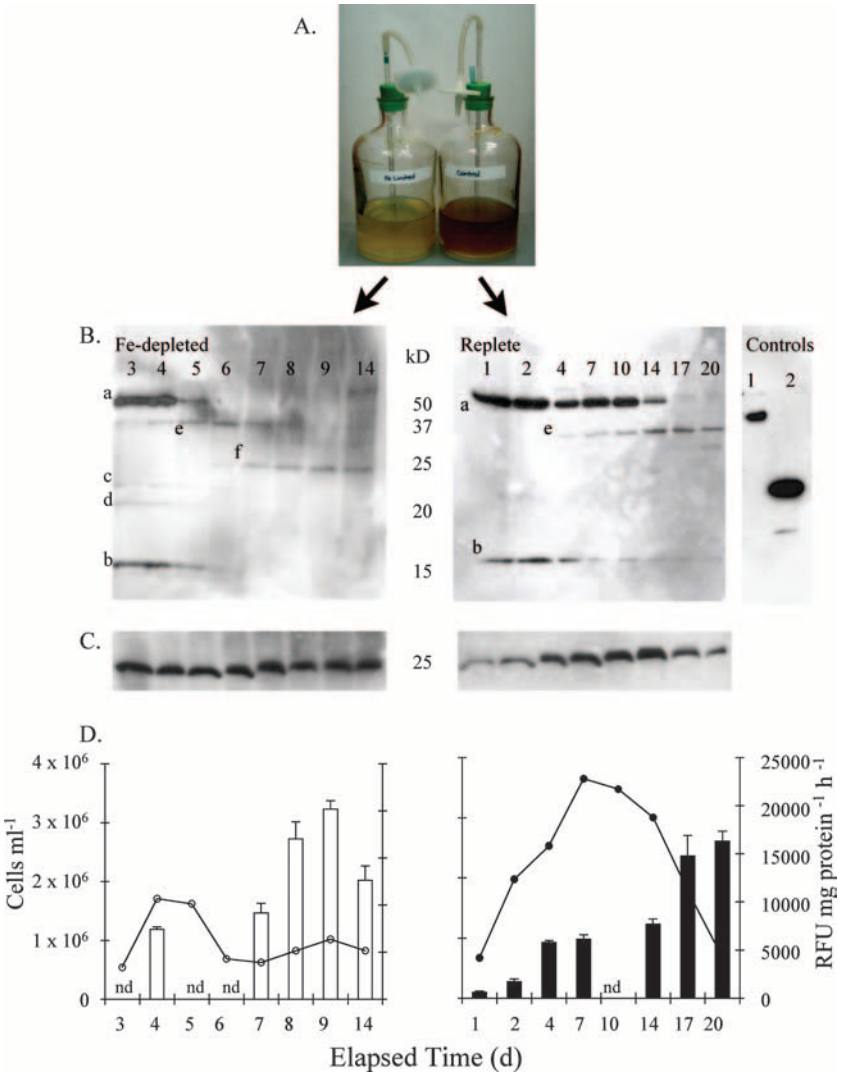

FIG. 6. (A) Visual comparison of *T. pseudonana* cells incubating in replete and Fe-starved treatments at 7 days. (B and C) Western blot analysis of *T. pseudonana* extracts collected over a 14- or 20-day time course, illustrating immunohybridization to a polyclonal antibody raised against a purified, recombinant *E. huxleyi* metacaspase protein (B) and polyclonal antisera raised against a purified, recombinant *T. pseudonana* Mn-SOD (C). The elapsed time (in days [d]) is indicated above each sample well. Cell extracts from healthy *E. huxleyi* cells (right panel, lane 1) and purified, recombinant human caspase 8 (right panel, lane 2) served as controls for EhMC probing. (D) Corresponding time course of cell abundance and caspase-specific activity. Error bars represent the standard deviations of technical triplicates. The experiment shown is typical of three experiments. nd, not determined.

ulations, making it ecologically relevant, but also access to its complete genome sequence (3) allows for the identification of putative components of the PCD molecular machinery.

Based on genome analyses, *T. pseudonana* possesses homologues to key components of the PCD biochemical machinery, including metacaspases, HtrA family proteases, apoptosis-associated nuclear factors (E2F and DP1), cell death suppressor proteins, and a cellular apoptosis susceptibility protein (43). At the same time, *T. pseudonana* lacks homologues of important elements of metazoan apoptotic pathways, such as p53 and the Bcl-2 family of apoptosis regulators, as well as Toll/interleukin-1 receptor (TIR) proteins or apoptotic adenosine triphosphatases (AP-ATPases), both of which are abundant in *Arabidopsis thaliana*. These findings raise fundamental questions about whether *T. pseudonana* possesses a functional PCD pathway and, if so, how it is regulated. Here, we focused on the involvement of metacaspases, given their ancestral relationship to caspases (10, 56) and their putative roles as PCD initiators and executioners. We specifically investigated the presence of metacaspase genes in *T. pseudonana*, their gene and protein expression in response to physiological stress, and their potential role in the implementation of PCD.

T. pseudonana displayed morphological and biochemical characteristics consistent with caspase-mediated PCD in response to Fe starvation and culture age. Morphological characteristics included extensive vacuolization and the internal degradation of organelles while maintaining cell membrane integrity. *T. pseudonana* cells also exhibited diagnostic biochemical markers of PCD, such as the externalization of PTS, measured via Annexin V staining, and caspase activation, mea-

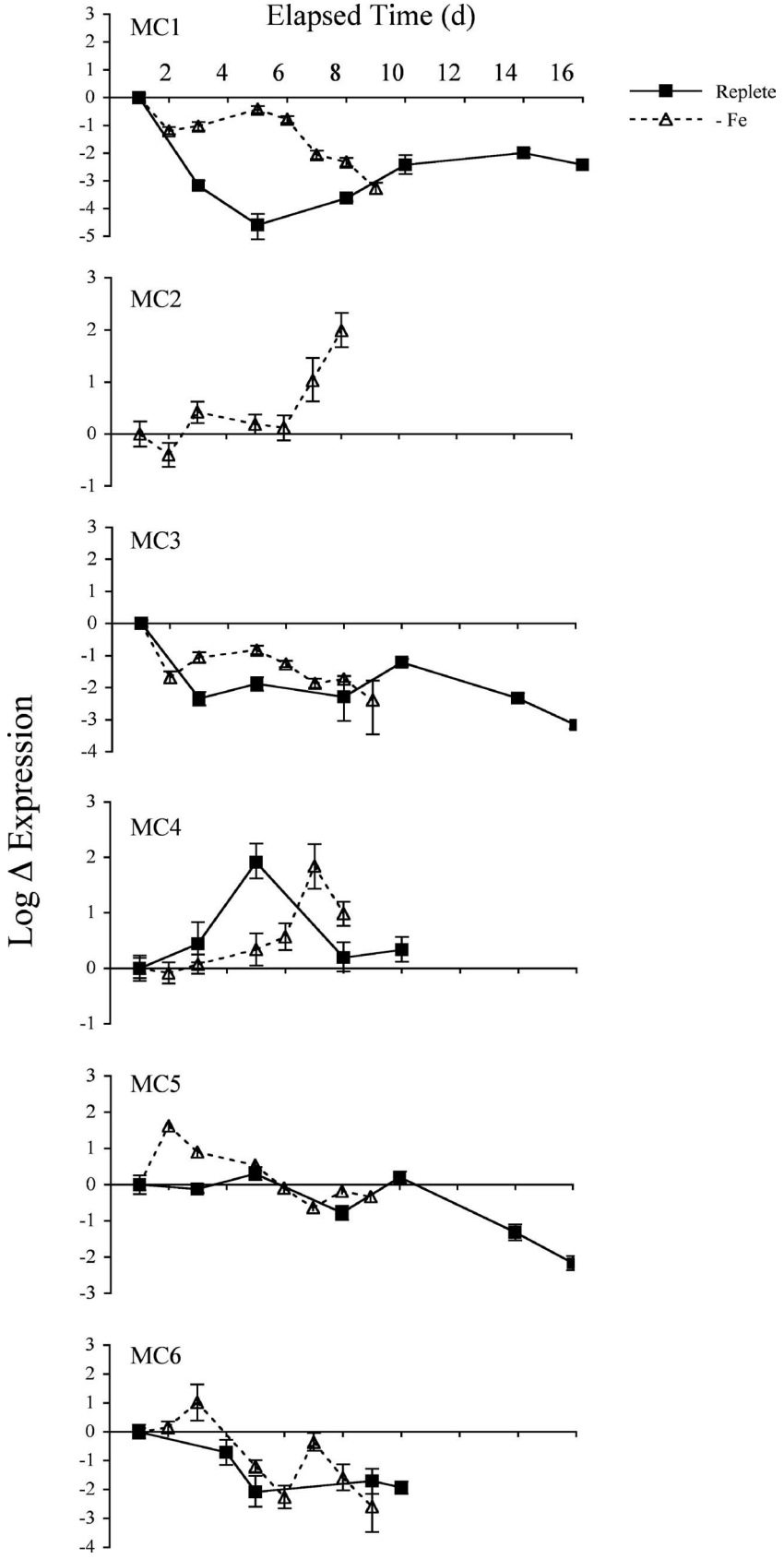

FIG. 7. Time course of TpMC gene expression for replete and Fe-starved treatments. Shown are the log fold changes in gene expression for each individual metacaspase gene, normalized to actin and calibrated to the first day (d) of the experiment. Data correspond to the culture and Western blotting dynamics shown in Fig. 6. A plot for TpMC2 expression is not shown for the replete culture due to undetectable expression. No expression was detected for TpMC6 in replete culture after 10 days. Error bars represent the standard deviations of technical triplicates. The experiment shown is typical of three experiments.

sured via the hydrolysis of the canonical fluorogenic peptide substrate for caspase 8, IETD-AFC. Elevated hydrolysis of DEVD-AFC, which has a higher specificity for caspase 3, also was observed but was <54% of the level of IETD-AFC hydrolysis. Direct staining of *T. pseudonana* cells with an FITC conjugate of the broad-spectrum caspase inhibitor z-VAD-FMK confirmed caspase activation. FITC–z-VAD-FMK freely diffuses into cells, binds to activated caspases, and serves as an in vivo marker. Effective staining of *T. pseudonana* was consistently observed for photosynthetically unhealthy cells, identified by their weak chlorophyll fluorescence. Furthermore, the activation of caspase activity strongly correlated with decreases in both the specific growth rate and photosynthetic efficiency, signifying that its induction was specific for stress and death.

Fe starvation triggered dramatic mortality, extensive internal degradation, and a very high level of caspase activity compared to that of aging cells in replete media. Approximately 60 to 70% of Fe-starved cells were positively stained with FITC–z-VAD-FMK and FITC-Annexin V, whereas only <20% of aging cultures were similarly stained. When caspase activity was plotted as a function of the mortality rate (per day) and the F_v/F_m, Fe-starved cells were characterized by steeper slopes, indicative of a stronger response at respective levels of physiological stress. Fe plays a critical role in phytoplankton growth, since it is required for photosynthetic electron transfer and reductive biosynthesis (30). Dramatic reductions in photosynthetic efficiency under Fe starvation signify uncoupled electron flow through photosystem II, ultimately leading to the production of ROS in oxygenic photoautotrophs (6), which in turn induces PCD (23, 60). Indeed, we found highly elevated expression of a chloroplast-localized, Mn-SOD (64) in Fe-starved cell extracts by using Western blot analysis, diagnostic of a subcellular response to elevated ROS (48, 64). PCD also has been observed under Fe starvation for the cyanobacterium *Trichodesmium* sp. strain IMS101 (6, 7) and the coccolithophore *E. huxleyi* (K. D. Bidle, unpublished data), suggesting it is a universal trigger of PCD among evolutionarily diverse phytoplankton. Interestingly, ROS and caspase activation in *Trichodesmium* spp. (7) and *T. pseudonana* (35) are coupled with the production of transparent exopolymeric particle production and aggregate formation, suggestive of a mechanistic role for PCD in influencing the vertical flux of organic matter in the oceans.

In the contemporary open ocean, Fe is drawn down to extremely low concentrations during late-phase phytoplankton blooms, leading to the physiological limitation of metabolic functions. Furthermore, Fe critically limits phytoplankton growth and primary productivity in high-nutrient low-chlorophyll areas such as the Southern Ocean and the equatorial Pacific (12, 21, 25, 26). Indeed, Coale et al. (25) documented a severe iron limitation of photosynthesis for in situ, open-ocean phytoplankton populations prior to iron fertilization, such that the F_v/F_m was very low (<0.25). A very low F_v/F_m also was reported for the equatorial Pacific (37) and for the Southern Ocean (12) high-nutrient low-chlorophyll zones. After iron enrichment, the F_v/F_m increased to >0.5, indicating a release from iron limitation. Even though open-ocean diatoms likely are better adapted to low-Fe conditions than coastal diatoms like *T. pseudonana*, they clearly experience severe physiological and photosynthetic stress under prevailing Fe concentrations. Our findings that a low F_v/F_m strongly triggers caspase activity suggest that Fe-limited zones represent a relevant ecological context for a biochemically active PCD machinery.

The characterization of PCD based solely on classic morphological features (36, 62) is inadequate for organisms with extensive evolutionary histories, including phytoplankton, which have an ~3 billion year evolutionary record and predate metazoans by >2 billion years (10, 29). Sperandio et al. (52) described an alternative type of PCD, termed paraptosis, in animal cells that fails to fulfill classic morphological and biochemical criteria for apoptosis, and they postulated that it may be particularly relevant for unicellular eukaryotic microorganisms with ancient origins. Paraptosis requires de novo gene expression and is characterized by increased vacuolization, caspase activation, and a lack of classic DNA fragmentation. However, it lacks critical biochemical features of apoptosis, most notably an insensitivity to caspase inhibitors like z-VAD-FMK and T-butyloxycarbonyl-Asp(*O-methyl*)-fluoromethyl ketone (BAF) (52). PCD in fission yeast (*Schizosaccharomyces pombe* [34]), slime mold (*Dictyostelium discoideum* [27]), and diverse lineages of prokaryotic and eukaryotic phytoplankton (e.g., cyanobacteria [6], chlorophytes [42, 51], dinoflagellates [32, 59, 60], and diatoms [*T. pseudonana]* [this study]) is characterized by cytoplasmic vacuolization and caspase activation in the absence of DNA laddering. In *T. pseudonana*, we clearly demonstrated that caspase activity was essential to PCD execution. The addition of z-VAD-FMK abolished caspase activity and temporarily rescued Fe-starved cells from PCD, instead allowing them to grow at reasonably high rates. A similar dependence of PCD on caspase activity has been observed for the coccolithophore *E. huxleyi* in response to viral infection (11), suggesting that phytoplankton PCD shares fundamental functional biochemistries with apoptosis.

The cellular roles and activities of metacaspases remain open questions regarding unicellular protists and plants. Their genetic signatures have been directly linked to caspase activity and the execution of PCD in yeast (41) and trypanosomes (53). In plants, metacaspases possess altered catalytic activity with higher specificity at arginine and lysine residues (13, 63), while in the protozoan parasites of the *Leishmania* genus they have trypsin-like activity. Nonetheless, in each case metacaspases have been shown to execute PCD. Metacaspases are widespread among prokaryotic and eukaryotic phytoplankton genomes (10), hinting at their early evolutionary development. Six metacaspase-like proteases were identified in the *T. pseudonana* genome, each containing conserved p20 caspase domains (e.g., peptidase_C14 and COG4249) and shared conserved amino acid sequences within the histidine-cysteine catalytic diad characteristic of caspases, metacaspases, and paracaspases (56). TpMCs were most similar to metacaspase-like proteins in several different fungi, supporting previous findings of a phylogenetic relatedness to unicellular protists and plants (10). TpMC3 contains a chloroplast transit peptide and likely is targeted to the chloroplast, hinting at a potential connection between metacaspases and the activation of PCD with the photosynthetic machinery. Lastly, there is a weak indication that TpMC2 is targeted to the mitochondria, which is well known to play an active role in triggering PCD. These findings suggest that although TpMCs share conserved amino acids and

caspase domain signatures, they appear to have unique subcellular localization and cellular roles.

A critical open question regarding phytoplankton metacaspases is whether they are expressed and function as PCD executioners. Metazoan caspases are constitutively expressed as procaspases and are posttranslationally cleaved and activated upon stress (55). Based on the available bioinformatics data in the *T. pseudonana* genome browser, ESTs have been detected for each metacaspase under various culture conditions (43). In order to assess metacaspase protein expression, we used a recently developed polyclonal antibody against a purified, recombinant EhMC. *E. huxleyi* (a prymnesiophyte of the class Haptophyceae) belongs to the coccolithophores, a class of unicellular phytoplankton that, along with diatoms, dominates the modern ocean (29). The EhMC antiserum previously was used to investigate the mechanistic link between PCD and viral infection by specifically examining metacaspase expression during a lytic viral infection of *E. huxleyi* (11). TpMCs showed significant amino acid identity to EhMC in partial alignments, most notably the histidine-cysteine-containing active-site regions, suitable for antibody recognition. Phylogenetic analysis of the caspase superfamily of proteins confirmed the relatedness of TpMCs and EhMCs, with both grouping with metacaspases from unicellular protists and plants (10). Lastly, the EhMC antibody displayed strong immunohybridization to purified, recombinant caspase 8 (11), revealing fundamental epitope conservation between EhMC and classic, metazoan caspases.

Distinct proteins in *T. pseudonana* cell extracts from Fe-starved and replete cultures hybridized with the EhMC antiserum, ranging in size from ~17 to ~50 kDa and corresponding to the predicted molecular masses of TpMC proteins in current gene models. Exponentially growing cells in both culture treatments constitutively expressed proteins consistent with the putative molecular masses of TpMC3 (Fig. 6B, band a) and TpMC6 (Fig. 6B, band b). These proteins generally persisted for up to 10 days in the replete culture but disappeared from the Fe-starved culture after 5 days. Their disappearance was accompanied by the appearance of distinct lower-molecular-mass proteins (~25 and 37 kDa) consistent with the putative molecular masses of TpMC1/TpMC4 (Fig. 6B, band e) and TpMC2/TpMC5 (Fig. 6B, band f), respectively. The proteins were present only in cell extracts with caspase-specific activity and during decreases in cell abundance (Fig. 6D). Given the strong epitope similarities between TpMCs and EhMCs, the lack of hybridization with preimmune serum, and the close correspondence between observed protein bands and predicted TpMC molecular masses, our data should accurately reflect TpMC protein expression.

qRT-PCR analyses generally revealed similar patterns of TpMC gene expression under Fe starvation and culture age, in which some TpMCs were regulated by physiological stress and correlated with caspase activity. The expression of five TpMC genes (TpMC1, TpMC3, TpMC4, TpMC5, and TpMC6) was detected in aging cells incubating in replete f/2 medium. Only TpMC4 expression was upregulated as the cells demonstrated PCD markers. All six TpMCs genes were expressed in Fe-starved cells, with TpMC2 and TpMC4 expression coinciding with reduced photosynthetic efficiency, caspase activation, and cell mortality. The expression of TpMC5 and TpMC6, while initially upregulated, subsequently dropped when cells were physiologically stressed. Our results demonstrate that while most metacaspases are constitutively expressed in healthy *T. pseudonana* cells, only a few are transcriptionally activated during PCD.

Overall, there was a close correlation between Western blotting and qRT-PCR results. Our findings suggest that metacaspases have diverse roles in diatoms. For example, we observed high, constitutive gene expression and protein abundances corresponding to TpMC1, TpMC3, TpMC5, and TpMC6 in actively growing *T. pseudonana* cells, along with subsequent decreases under physiological stress and death. Given the low level of caspase-specific activity observed in healthy *T. pseudonana* cells, these metacaspases likely do not possess caspase activity and are not responsible for PCD execution. Rather, our data are consistent with housekeeping functions. High, constitutive metacaspase expression has been observed in the coccolithophore *E. huxleyi* (11), the diatom *Phaeodactylum tricornutum* (A. Vardi, unpublished data), and the cyanobacterium *Trichodesmium erythraeum* (K. D. Bidle, unpublished). On the other hand, we observed elevated, late-phase gene and protein expression for TpMC2 and TpMC4. Their close correspondence with photosynthetic stress, elevated caspase-specific activity, and PCD markers suggests that these metacaspases function as PCD executioners and possess caspase activity. This needs to be confirmed and further elucidated using recently developed reverse genetic approaches (49).

To our knowledge, this is the first study to experimentally investigate the expression and putative roles of metacaspases in marine diatoms. Our findings significantly improve on previous reports of metacaspase identity in *T. pseudonana* (43). *T. pseudonana* clearly possesses the core execution machinery anchored around the expression and activation of specific metacaspases, but their individual roles are uncharacterized. Elucidating the ecological and evolutionary roles of PCD in *T. pseudonana* requires a more extensive mechanistic understanding of how it activates, regulates, and executes PCD in response to a variety of stressors. For example, observations of relatively low levels of caspase activity induced by phosphorus starvation compared to that induced by iron starvation (7 and data not shown) suggest differential activation and regulation of the PCD machinery. Unfortunately, the biochemical complexity and regulation of *T. pseudonana's* PCD machinery currently are unknown. *T. pseudonana* does possess a homologous protein (Protein ID 11118; BLASTp E value of 1×10^{-55}) to *S. costatum* ScDSP (GenBank accession no. AAY27742) with conserved EF-hand calcium binding motifs (cd00051 and COG5126). We hypothesize that this protein serves to couple stress signals to the PCD execution machinery. Indeed, the timing of PCD activation in *T. pseudonana* (this study) closely parallels the timing of increased Sc*DSP* gene expression during death in *S. costatum* (24). Together with recent discoveries that chemical signals and secondary metabolites (i.e., dissolved thiol proteases, aldehydes, nitric oxide, and calcium) elicit PCD in phytoplankton (22, 60, 61), our findings provide a novel mechanistic context for algal bloom dynamics in response to biotic stressors (i.e., nutrient depletion, age, and viral infection). Future investigations should address the potential link between putative death regulators and metacaspases in

order to reveal how PCD is activated in these unicellular photoautotrophs.

ACKNOWLEDGMENTS

We thank Valentin Starovoytov for TEM analysis, Liti Haramaty and Matthew Oliver for laboratory assistance, and Kim Thamatrakoln and Assaf Vardi for valuable discussions. We are especially grateful to Adam Kustka and Paul Field for their assistance with trace Fe analyses. The comments from three anonymous reviewers significantly strengthened the manuscript.

This work was supported by National Science Foundation grant IOB-0414536 to K.D.B. and by funds from the Rutgers College Honors Program to S.J.B.

REFERENCES

1. **Agustí, S., and M. C. Sánchez.** 2002. Cell viability in natural phytoplankton communities quantified by a membrane permeability probe. Limnol. Oceanogr. **47:**818–828.
2. **Agustí, S., M. P. Satta, M. P. Mura, and E. Benavent.** 1998. Dissolved esterase activity as a trace of phytoplankton lysis: Evidence of high phytoplankton lysis rates in the northwestern Mediterranean. Limnol. Oceanogr. **43:**1836–1849.
3. **Armbrust, E. V., J. A. Berges, C. Bowler, B. R. Green, D. Martinez, N. H. Putnam, S. Zhou, A. E. Allen, K. E. Apt, M. Bechner, M. A. Brzezinski, B. K. Chaal, A. Chiovitti, A. K. Davis, M. S. Demarest, J. C. Detter, T. Glavina, D. Goodstein, M. Z. Hadi, U. Hellsten, M. Hildebrand, B. D. Jenkins, J. Jurka, V. V. Kapitonov, N. Kröger, W. W. Y. Lau, T. W. Lane, F. W. Larimer, J. C. Lippmeier, S. Lucas, M. Medina, A. Montsant, M. Obornik, M. Schnitzler-Parker, B. Palenik, G. J. Pazour, P. M. Richardson, T. A. Rynearson, M. A. Saito, D. C. Schwartz, K. Thamatrakoln, K. Valentin, A. Vardi, F. P. Wilkerson, and D. S. Rokhsar.** 2004. The genome of the diatom *Thalassiosira pseudonana*: Ecology, evolution and metabolism. Science **306:**79–86.
4. **Azam, F.** 1986. Nutrient cycling and food web dynamics in the Southern California Bight: the microbial food web, p. 274–288. *In* R. W. Eppley (ed.), Plankton dynamics of the southern California bight. Lecture notes on coastal and estuarine studies, vol. 15. Springer-Verlag, Berlin, Germany.
5. **Berges, J. A., and P. G. Falkowski.** 1998. Physiological stress and cell death in marine phytoplankton: induction of proteases in response to nitrogen or light limitation. Limnol. Oceanogr. **43:**129–135.
6. **Berman-Frank, I., K. Bidle, L. Haramaty, and P. Falkowski.** 2004. The demise of the marine cyanobacterium, Trichodesmium spp., via an autocatalyzed cell death pathway. Limnol. Oceanogr. **49:**997–1005.
7. **Berman-Frank, I., G. Rosenberg, O. Levitan, L. Haramaty, and X. Mari.** 2007. Coupling between autocatalytic cell death and transparent exopolymeric particle production in the marine cyanobacterium Trichodesmium. Environ. Microbiol. **9:**1415–1422.
8. **Bidle, K. D., and F. Azam.** 1999. Accelerated dissolution of diatom silica by natural marine bacterial assemblages. Nature **397:**508–512.
9. **Bidle, K. D., M. A. Brzezinski, R. A. Long, J. Jones, and F. Azam.** 2003. Diminished efficiency in the oceanic silica pump caused by bacteria-mediated silica dissolution. Limnol. Oceanogr. **48:**1855–1868.
10. **Bidle, K. D., and P. G. Falkowski.** 2004. Cell death in planktonic photosynthetic microorganisms. Nat. Rev. Microbiol. **2:**643–655.
11. **Bidle, K. D., L. Haramaty, J. Barcelos-Ramos, and P. G. Falkowski.** 2007. Viral activation and recruitment of metacaspases in the unicellular coccolithophorid, Emiliania huxleyi. Proc. Natl. Acad. Sci. USA **104:**6049–6054.
12. **Boyd, P. W., A. J. Watson, C. S. Law, E. R. Abraham, T. Trull, R. Murdoch, D. C. E. Bakker, A. R. Bowie, K. O. Buesseler, H. Chang, M. Charette, P. Croot, K. Downing, R. Frew, M. Gall, M. Hadfield, J. Hall, M. Harvey, G. Jameson, J. LaRoche, M. Liddicoat, R. Ling, M. T. Maldonado, R. M. McKay, S. Nodder, S. Pickmere, R. Pridmore, S. Rintoul, K. Safi, P. Sutton, R. Strzepek, K. Tanneberger, S. Turner, A. Waite, and J. Zeldis.** 2000. A mesoscale phytoplankton bloom in the polar Southern Ocean stimulated by iron fertilization. Nature **407:**695–702.
13. **Bozhkov, P. V., M. F. Suarez, L. H. Filonova, G. Daniel, A. A. Zamyatnin, Jr., S. Rodriguez-Nieto, B. Zhivotovsky, and A. Smertenko.** 2005. Cysteine protease mcII-Pa executes programmed cell death during plant embryogenesis. Proc. Natl. Acad. Sci. USA **102:**14463–14468.
14. **Bratbak, G., J. K. Egge, and M. Heldal.** 1993. Viral mortality of the marine alga Emiliania huxleyi (Haptophyceae) and termination of algal blooms. Mar. Ecol. Prog. Ser. **93:**39–48.
15. **Brussaard, C. P. D., A. A. M. Noordeloos, and R. Riegman.** 1997. Autolysis kinetics of the marine diatom *Ditylum brightwellii* (Bacillariophyceae) under nitrogen and phosphorus limitation and starvation. J. Phycol. **33:**980–987.
16. **Brussaard, C. P. D., R. Riegman, A. A. M. Noordeloos, G. C. Cadée, H. Witte, A. J. Kop, G. Nieuwland, F. C. V. Duyl, and R. P. M. Bak.** 1995. Effects of grazing, sedimentation and phytoplankton cell lysis on the structure of a coastal pelagic food web. Mar. Ecol. Prog. Ser. **123:**259–271.
17. **Brzezinski, M. A., J. Jones, K. Bidle, and F. Azam.** 2003. The balance between silica production and silica dissolution in the sea. Insights from Monterey Bay, California applied to the global data set. Limnol. Oceanogr. **48:**1846–1854.
18. **Brzezinski, M. A., and D. M. Nelson.** 1989. Seasonal changes in the silicon cycle within a Gulf Stream warm-core ring. Deep-Sea Res. **36:**1009–1030.
19. **Brzezinski, M. A., and D. M. Nelson.** 1995. The annual silica cycle in the Sargasso Sea near Bermuda. Deep-Sea Res. **42:**1215–1237.
20. **Brzezinski, M. A., D. R. Phillips, F. P. Chavez, G. E. Friederich, and R. C. Dugdale.** 1997. Silica production in the Monterey, California, upwelling system. Limnol. Oceanogr. **42:**1694–1705.
21. **Buesseler, K. O., J. E. Andrews, S. M. Pike, and M. A. Charette.** 2004. The effects of iron fertilization on carbon sequestration in the Southern Ocean. Science **304:**414–417.
22. **Casotti, R., S. Mazza, C. Brunet, V. Vantrepotte, and A. Ianora.** 2005. Growth inhibition and toxicity of the diatom aldehyde 2-trans, 4-trans-decadienal on Thalassiosira weissflogii (Bacillariophyceae). J. Phycol. **41:**7–20.
23. **Chandra, J., A. Samali, and S. Orrenius.** 2000. Triggering and modulation of apoptosis by oxidative stress. Free Rad. Biol. Med. **29:**323–333.
24. **Chung, C.-C., S.-P. Hwang, and J. Chang.** 2005. Cooccurence of Sc*DSP* gene expression, cell death, and DNA fragmentation in a marine diatom, *Skeletonema costatum*. Appl. Environ. Microbiol. **71:**8744–8751.
25. **Coale, K. H., K. S. Johnson, F. P. Chavez, K. O. Buesseler, R. T. Barber, M. A. Brzezinski, W. P. Cochlan, F. J. Millero, P. G. Falkowski, J. E. Bauer, R. H. Wanninkhof, R. M. Kudela, M. A. Altabet, B. E. Hales, T. Takahashi, M. R. Landry, R. R. Bidigare, X. Wang, Z. Chase, P. G. Strutton, G. E. Friederich, M. Y. Gorbunov, V. P. Lance, A. K. Hilting, M. R. Hiscock, M. Demarest, W. T. Hiscock, K. F. Sullivan, S. J. Tanner, R. M. Gordon, C. N. Hunter, V. A. Elrod, S. E. Fitzwater, J. L. Jones, S. Tozzi, M. Koblizek, A. E. Roberts, J. Herndon, J. Brewster, N. Ladizinsky, G. Smith, D. Cooper, D. Timothy, S. L. Brown, K. E. Selph, C. C. Sheridan, B. S. Twining, and Z. I. Johnson.** 2004. Southern Ocean iron enrichment experiment: carbon cycling in high- and low-Si waters. Science **304:**408–414.
26. **Coale, K. H., K. S. Johnson, S. E. Fitzwater, R. M. Gordon, S. Tanner, F. P. Chavez, L. Ferioli, C. Sakamoto, P. Rogers, F. Millero, and others.** 1996. A massive phytoplankton bloom induced by an ecosystem-scale iron fertilization experiment in the equatorial Pacific Ocean. Nature **383:**495–501.
27. **Cornillon, S., C. Foa, J. Davoust, N. Buonavista, J. D. Gross, and P. Golstein.** 1994. Programmed cell death in *Dictyostelium*. J. Cell Sci. **107:** 2691–2704.
28. **Dugdale, R. C., and F. P. Wilkerson.** 1998. Silicate regulation of new production in the equatorial Pacific upwelling. Nature **391:**270–273.
29. **Falkowski, P. G., M. E. Katz, A. H. Knoll, A. Quigg, J. A. Raven, O. Schofield, and F. J. R. Taylor.** 2004. The evolution of modern eukaryotic phytoplankton. Science **305:**354–360.
30. **Falkowski, P. G., and J. A. Raven.** 2007. Aquatic photosynthesis, 2nd ed. Princeton University Press, Princeton, NJ.
31. **Field, C. B., M. J. Behrenfeld, J. T. Randerson, and P. Falkowski.** 1998. Primary production of the biosphere: integrating terrestrial and oceanic components. Science 237–240.
32. **Franklin, D. J., and J. A. Berges.** 2004. Mortality in cultures of the dinoflagellate Amphidinium carterae during culture senescence and darkness. Proc. Biol. Sci. **271:**2099–2107.
33. **Guillard, R. R. L.** 1975. Culture of phytoplankton for feeding marine invertebrates, p. 26–60. *In* W. L. Smith and M. H. Chanley (ed.), Culture of marine invertebrate animals. Plenum Press, New York, NY.
34. **Jürgensmeier, J. M., S. Krajewski, R. C. Armstrong, G. M. Wilson, T. Oltersdorf, L. C. Fritz, J. C. Reed, and S. Ottilie.** 1997. Bax- and Bak-induced cell death in the fission yeast *Schizosaccharomyces pombe*. Mol. Biol. Cell **8:**325–339.
35. **Kahl, L. A., A. Vardi, and O. Schofield.** 2008. Effects of phytoplankton physiology on export flux. Mar. Ecol. Prog. Ser. **354:**1–6.
36. **Kerr, J. F. R., A. H. Wyllie, and A. R. Currie.** 1972. Apoptosis: a basic biological phenomenon with wide ranging implications. Br. J. Cancer **26:** 239–257.
37. **Kolber, Z. S., R. T. Barber, K. H. Coale, S. E. Fitzwater, R. M. Greene, K. S. Johnson, S. Lindley, and P. G. Falkowski.** 1994. Iron limitation of phytoplankton photosynthesis in the equatorial Pacific Ocean. Nature **371:**145–149.
38. **Kolber, Z. S., O. Prasil, and P. G. Falkowski.** 1998. Measurements of variable chlorophyll fluorescence using fast repetition rate techniques: defining methodology and experimental protocols. Biochim. Biophys. Acta **1367:**88–106.
39. **Kustka, A. B., A. E. Allen, and F. M. M. Morel.** 2007. Sequence analysis and transcriptional regulation of iron acquisition genes in two marine diatoms. J. Phycol. **43:**715–729.
40. **Longhurst, A. R., and W. G. Harrison.** 1989. The biological pump: profiles of plankton production and consumption in the upper ocean. Progr. Oceanogr. **22:**47–123.
41. **Madeo, F., E. Herker, C. Maldener, S. Wissing, S. Lächelt, M. Herlan, M. Fehr, K. Lauber, S. J. Sigrist, S. Wesselborg, and K.-U. Fröhlich.** 2002. A caspase-related protease regulates apoptosis in yeast. Mol. Cell **9:**911–917.

42. **Moharikar, S., J. S. D'Souza, A. B. Kulkarni, and B. J. Rao.** 2006. Apoptotic-like cell death pathway is induced in unicellular chlorophyte Chlamydomonas reinhardtii (Chlorophyceae) cells following UV irradiation: detection and functional analyses. J. Phycol. **42:**423–433.
43. **Montsant, A., A. E. Allen, S. Coesel, A. D. Martino, A. Falciatore, M. Heijde, K. Jabbari, U. Maheswari, M. Mangogna, E. Rayko, M. Siaut, A. Vardi, K. E. Apt, J. A. Bergesf, A. Chiovitti, A. K. Davis, M. Z. Hadii, T. W. Lane, J. C. Lippmeier, D. Martinez, M. S. Parker, G. J. Pazour, M. A. Saitop, K. Thamatrakoln, D. S. Rokhsar, E. V. Armbrust, and C. Bowler.** 2007. Identification and comparative genomic analysis of signaling and regulatory components in the diatom Thalassiosira pseudonana. J. Phycol. **43:**585–604.
44. **Nelson, D. M., and J. J. Goering.** 1977. Near-surface silica dissolution in the upwelling region off northwest Africa. Deep-Sea Res. **24:**65–73.
45. **Nelson, D. M., J. J. Goering, and D. W. Boisseau.** 1981. Consumption and regeneration of silicic acid in three coastal upwelling systems, p. 242–256. *In* F. A. Richards (ed.), Coastal upwelling. American Geophysical Union, Washington, DC.
46. **Nelson, D. M., and L. I. Gordon.** 1982. Production and pelagic dissolution of biogenic silica in the Southern Ocean. Geochim. Cosmochim. Acta **46:**491–501.
47. **Nelson, D. M., P. Tréguer, M. A. Brzezinski, A. Leynaert, and B. Quéguiner.** 1995. Production and dissolution of biogenic silica in the ocean: revised global estimates, comparison with regional data and relationship to biogenic sedimentation. Global Biogeochem. Cycles **9:**359–372.
48. **Peers, G., and N. M. Price.** 2004. A role for manganese in superoxide dismutases and growth of iron-deficient diatoms. Limnol. Oceanogr. **49:** 1774–1783.
49. **Poulsen, N., P. M. Chesley, and N. Kröger.** 2006. Molecular genetic manipulation of the diatom Thalassiosira pseudonana (Bacillariophyceae). J. Phycol. **42:**1059–1065.
50. **Ragueneau, O., S. Schultes, K. Bidle, P. Claquin, and B. Moriceau.** 2006. Si and C interactions in the world ocean: importance of ecological processes and implications for the role of diatoms in the biological pump. Global Biogeochem. Cycles **20:**GB4502.
51. **Segovia, M., L. Haramaty, J. A. Berges, and P. G. Falkowski.** 2003. Cell death in the unicellular chlorophyte *Dunaliella tertiolecta*: a hypothesis on the evolution of apoptosis in higher plants and metazoans. Plant Physiol. **132:** 99–105.
52. **Sperandio, S., I. D. Belle, and D. E. Bredesen.** 2000. An alternative, non-apoptotic form of programmed cell death. Proc. Natl. Acad. Sci. USA **97:** 14376–14381.
53. **Szallies, A., B. K. Kubata, and M. Duszenko.** 2002. A metacaspase of *Trypanosoma brucei* causes loss of respiration competence and clonal death in the yeast *Saccharomyces cerevisiae*. FEBS Lett. **517:**144–150.
54. **Thellin, O., W. Zorzi, B. Lakaye, B. DeBorman, B. Coumans, G. Hennen, T. Grisar, A. Igout, and E. Heinen.** 1999. Housekeeping genes as internal standards: use and limits. J. Biotechnol. **75:**291–295.
55. **Thornberry, N. A., and Y. Lazebnik.** 1998. Caspases: enemies within. Science **281:**1312–1316.
56. **Uren, A. G., K. O'Rourke, M. T. Pisabarro, S. Seshagiri, E. V. Koonin, and V. M. Dixit.** 2000. Identification of paracaspases and metacaspases: two ancient families of caspase-like proteins, one of which plays a key role in MALT lymphoma. Mol. Cell **6:**961–967.
57. **Valiela, I.** 1995. Marine ecological processes. Springer-Verlag, New York, NY.
58. **van Boekel, W. H. M., F. C. Hansen, R. Riegman, and R. P. M. Bak.** 1992. Lysis-induced decline of a Phaeocystis spring bloom and coupling with the microbial foodweb. Mar. Ecol. Prog. Ser. **81:**269–276.
59. **Vardi, A., I. Berman-Frank, T. Rozenberg, O. Hadas, A. Kaplan, and A. Levine.** 1999. Programmed cell death of the dinoflagellate *Peridinium gatunense* is mediated by CO_2 limitation and oxidative stress. Curr. Biol. **9:**1061–1064.
60. **Vardi, A., D. Eisenstadt, O. Murik, I. Berman-Frank, T. Zohary, A. Levine, and A. Kaplan.** 2007. Synchronization of cell death in a dinoflagellate population is mediated by an excreted thiol protease. Environ. Microbiol. **9:**360–369.
61. **Vardi, A., F. Formiggini, R. Casotti, A. deMartino, F. Ribalet, A. Miralto, and C. Bowler.** 2006. A stress surveillance system based on calcium and nitric oxide in marine diatoms. PLoS Biol. **4:**e60.
62. **Walker, N. I., B. V. Harmon, G. C. Gobé, and J. F. R. Kerr.** 1988. Patterns of cell death, p. 18–54. *In* G. Jasmin (ed.), Kinetics and patterns of necrosis, vol. 13. Karger, Basel, Switzerland.
63. **Watanabe, N., and E. Lam.** 2005. Two *Arabidopsis* metacaspases AtMCP1b and AtMCP2b are arginine/lysine-specific cysteine proteases and activate apoptosis-like cell death in yeast. J. Biol. Chem. **280:**14691–14699.
64. **Wolfe-Simon, F., V. Starovoytov, J. R. Reinfelder, O. Schofield, and P. G. Falkowski.** 2006. Localization and role of manganese superoxide dismutase in marine diatoms. Plant Physiol. **142:**1701–1709.